

# Reconcile the AMS-02 positron fraction and Fermi-LAT/HESS total $e^\pm$ spectra by the primary electron spectrum hardening

Qiang Yuan<sup>a,b</sup> and Xiao-Jun Bi<sup>b</sup>

<sup>a</sup>Key Laboratory of Dark Matter and Space Astronomy, Purple Mountain Observatory,  
Chinese Academy of Sciences, Nanjing 210008, P.R.China

<sup>b</sup>Key Laboratory of Particle Astrophysics, Institute of High Energy Physics,  
Chinese Academy of Science, P.O.Box 918-3, Beijing 100049, P.R.China

(Dated: October 10, 2018)

The recently reported positron fraction up to  $\sim 350$  GeV by AMS-02 seems to have tension with the total electron/positron spectra detected by Fermi and HESS, for either pulsar or dark matter annihilation/decay scenario as the primary positron sources. In this work we will show that the tension will be removed by an adjustment of the primary electron spectrum. If the primary electron spectrum becomes harder above  $\sim 50$  GeV, similar as the cosmic ray nuclei spectrum, the AMS-02 positron fraction and Fermi/HESS data can be well fitted by both the pulsar and dark matter models. This result may be suggestive of a common origin of the cosmic ray nuclei and the primary electrons. Furthermore, this study also implies that the properties of the extra sources derived from the fitting to the AMS-02 data should depend on the form of background.

PACS numbers: 96.50.S-

## I. INTRODUCTION

The AMS-02 collaboration reported the very precise measurement of the positron fraction  $e^+/e^\pm$  with energies up to 350 GeV recently [1]. The positron fraction shows a continuous increase up to  $\sim 100$  GeV, which is consistent with the previous PAMELA result [2, 3] and is lower than that measured with Fermi-LAT [4]. A flattening of the positron fraction above  $\sim 100$  GeV is revealed by the AMS-02 data, for the first time. The AMS-02 data implies that there is excess of positrons above tens of GeV compared with the standard cosmic ray (CR) background, and the amount of excess positrons should be less than previously estimated according to the PAMELA data.

Several works appear to explain the AMS-02 data with pulsars [5] or dark matter (DM) scenarios [6–8]. A thorough study of the properties of the extra positron sources, including the astrophysical one like pulsars and the dark matter (DM) scenario, based on the AMS-02 data and the electron (or  $e^\pm$ ) spectra measured by PAMELA [9], Fermi-LAT [10, 11] and HESS [12, 13], was given shortly after the publication of the AMS-02 data [14] (Paper I). It was found that there was difficulty to fit the AMS-02 positron data and the Fermi-LAT/HESS total electron spectra simultaneously, either in the pulsar scenario or in the DM scenario. The results seem to imply that there might be *tension* between the AMS-02 data and the Fermi-LAT/HESS data, in the present theoretical framework. This conclusion has been confirmed by other studies<sup>1</sup> [16, 17]. One possible reason leading

to the *tension* is the constraint on the electron injection parameters by the pure electron spectrum by PAMELA. If the PAMELA data are not included, the primary electron spectrum has larger free space and the AMS-02 data and Fermi data can be easier to be fitted simultaneously, as shown in some recent works to explain the AMS-02 result [5–8].

Several possibilities to reconcile these two data sets were discussed in Paper I, including multiple components of the extra sources and the existence of spectral hardening of the primary electron spectrum. The idea to introduce a spectrum hardening of primary electrons to fit the data was also raised in [16, 18]. The spectrum hardening was stimulated by the observed spectral hardening of the nuclei spectra in recent years by several collaborations<sup>2</sup> [19–21]. A unified spectral hardening at rigidity  $R \sim 200$  GV (or  $E_k \sim 200$  GeV/n) was measured precisely by PAMELA or CREAM [20, 21]. If there is a spectral hardening of the CR nuclei spectra, it is natural to expect a similar hardening of the primary electron spectrum.

Models to explain the spectral hardening include the multi-component sources [22–26], non-linear acceleration of the particles [27], or the propagation effect [28, 29]. In

---

smaller [15]. The discussion of the present work may hold given the new AMS-02  $e^\pm$  spectra, since we study to reconcile the high energy behavior of Fermi-LAT data with the AMS-02 positron fraction.

<sup>2</sup> Note, however, the recent reported preliminary data about the proton and Helium spectra show no significant hardening as observed by PAMELA [15]. Whether or not the heavier nuclei have the hardening still needs to be tested by the future AMS-02 data. Since the present work is based on the electron and positron data, the AMS-02 results about the nuclei spectra have only a slight modification of the secondary positron spectrum and do not affect the discussion significantly.

---

<sup>1</sup> Also the preliminary data about the total  $e^\pm$  spectra by AMS-02 show the discrepancy with Fermi-LAT data below  $\sim 100$  GeV. For  $E \gtrsim 100$  GeV the difference between these two data sets are

[18] the authors pointed out that if there was a spectral hardening of the primary electron spectrum, there would be a less steep increase (or decrease) of the positron fraction above  $\sim 200$  GeV.

In the work we investigate in detail whether to involve such a spectral hardening of the primary electron spectrum can help eliminate the *tension* between the AMS-02 data and the Fermi-LAT/HESS data. We employ the CosRayMC tool developed in [30] to fit the observational data within the high dimensional parameter space. The GALPROP package<sup>3</sup> [31] to calculate the propagation of the charged CRs has been embedded in the Markov Chain Monte Carlo (MCMC) algorithm, which is well known to be efficient for the survey of high-dimensional correlated parameter space [32], in CosRayMC. The diffusion-reacceleration propagation frame is adopted, and the major propagation parameters are  $D_0|_{R_0=4\text{GV}} = 5.94 \times 10^{28} \text{ cm}^2 \text{ s}^{-1}$ ,  $\delta = 0.377$ ,  $v_A = 36.4 \text{ km s}^{-1}$  and  $z_h = 4.04 \text{ kpc}$  [33]. The goodness of fit, constraints and implication of the model parameters are discussed.

In the next Section we simply describe the models to fit the data. The results are presented in Sec. III. In Sec. IV we give the discussions and conclusions.

## II. MODEL

In this section we describe the major aspects of the theoretical models to reproduce the electron/positron data briefly. The injection spectra of the primary protons (heavier nuclei are less important in this study) and electrons are both assumed to be broken power-law functions with respect to momentum  $p$

$$q(p) \propto \begin{cases} (p/p_{\text{br},1}^{p,e})^{-\gamma_0}, & p < p_{\text{br},1}^{p,e} \\ (p/p_{\text{br},1}^{p,e})^{-\gamma_1}, & p_{\text{br},1}^{p,e} < p < p_{\text{br},2}^{p,e} \\ (p/p_{\text{br},2}^{p,e})^{-\gamma_2} (p_{\text{br},2}^{p,e}/p_{\text{br},1}^{p,e})^{-\gamma_1}, & p > p_{\text{br},2}^{p,e} \end{cases} \quad (2)$$

where  $p_{\text{br},1}$  represents the low energy break,  $p_{\text{br},2}$  is the high energy break to be responsible for the spectral hardening,  $\gamma_0$ ,  $\gamma_1$  and  $\gamma_2$  are the spectral indices in different momentum ranges. We also employ the log-parabolic function to describe the spectral hardening of the electrons, i.e.,  $q(p) \propto (p/p_{\text{br},1}^e)^{-\gamma_1 + \gamma_2 \log(p/\text{MeV})}$  for  $p > p_{\text{br},1}^e$ . In this case  $p_{\text{br},2}^e$  is not used. The absolute fluxes of protons and electrons are determined through normalizing the propagated fluxes to normalization factors  $A_p$  and  $A_e$ .

The background positrons are expected to be produced through the collision of CR nuclei with the interstellar medium (ISM) during the propagation. The parameterization of  $pp$  collision in [34] is employed to calculate the secondary production of positrons and electrons. Similar

as done in Paper I, we further introduce a free factor  $c_{e+}$  to adjust the absolute fluxes of the secondary positrons and electrons to fit the data. Such a factor may represent the uncertainties of the hadronic interactions, propagation models, the ISM density distributions, and the nuclear enhancement factor from heavy elements.

In the PAMELA era it was found that the background contribution are not enough to explain the observed positron fraction and total  $e^\pm$  data [35, 36]. Therefore the extra sources of  $e^\pm$  beyond the traditional CR background are introduced to explain the data. We will base on the same theoretical framework to fit the AMS-02 data in the work, assuming continuously distributed pulsars or the DM annihilation/decay to be the extra sources of  $e^\pm$ .

The injection spectrum of  $e^\pm$  from pulsars is assumed to be power-law with an exponential cutoff

$$q(p) = A_{\text{psr}} p^{-\alpha} \exp(-p/p_c), \quad (2)$$

where  $A_{\text{psr}}$  is the normalization factor,  $\alpha$  is the spectral index and  $p_c$  is the cutoff momentum. The spectral index  $\alpha$  is limited in the range 1.4 to 2.2 according to the  $\gamma$ -ray observations of pulsars [37]. The spatial distribution of pulsars is taken to be the cylindrically symmetric form given in [38]

$$f(R, z) \propto \left(\frac{R}{R_\odot}\right)^{2.35} \exp\left[-\frac{5.56(R - R_\odot)}{R_\odot}\right] \exp\left(-\frac{|z|}{z_s}\right), \quad (3)$$

where  $R_\odot = 8.5 \text{ kpc}$  is the distance of the solar location to the Galactic center,  $z_s \approx 0.2 \text{ kpc}$  is the characteristic height of the Galactic disk.

As for DM scenario (taking annihilation as illustration), we focus on the leptonic two-body annihilation channels  $\mu^+\mu^-$  and  $\tau^+\tau^-$ , as implied according to the PAMELA and Fermi-LAT/HESS data of the electrons/positrons and the antiprotons [39–41]. The positron/electron production function from DM annihilation is (assumed to be Majorana particles)

$$q(r, p) = \frac{\langle\sigma v\rangle}{2m_\chi^2} \frac{dN}{dp} \times \rho^2(r), \quad (4)$$

where  $m_\chi$  is the mass of DM particle,  $\langle\sigma v\rangle$  is the velocity weighted annihilation cross section,  $dN/dp$  is the yield spectrum for one annihilation of a pair of DM particles, and  $\rho(r)$  is the DM density profile. The spatial profile of DM energy density is taken to be Navarro-Frenk-White (NFW, [42]) distribution

$$\rho(r) = \frac{\rho_s}{(r/r_s)(1 + r/r_s)^2}, \quad (5)$$

with parameters  $r_s = 20 \text{ kpc}$  and  $\rho_s = 0.26 \text{ GeV cm}^{-3}$ .

For low energy particles we further employ a simple force field approximation to take into account the solar modulation effect [43]. Since the operation period of PAMELA and AMS-02 is close to the solar minimum, the modulation potential is required to be smaller than 1

<sup>3</sup> <http://galprop.stanford.edu/>

GV. Note, however, the low energy part of the positron fraction measured by PAMELA and AMS-02 might not be reproduced with such single solar modulation model, and more complicated charge-sign dependent modulation effect is necessary [44, 45].

### III. RESULTS

We first determine the parameters of the proton injection spectrum through fitting to the PAMELA [20] and CREAM [21] data. For CREAM data we include 10% systematic uncertainties as discussed in [21]. The high energy break  $p_{\text{br},2}^p$  is fixed to be 230 GeV as suggested by the PAMELA data. The best fitting parameters of the proton spectrum are:  $\gamma_0 = 1.80$ ,  $\gamma_1 = 2.42$ ,  $\gamma_2 = 2.33$ ,  $p_{\text{br},1}^p = 12.3$  GeV, and solar modulation potential  $\phi = 495$  MV. The normalization of the propagated proton flux at 100 GeV is  $A_p = 4.55 \times 10^{-9}$   $\text{cm}^{-2}\text{s}^{-1}\text{sr}^{-1}\text{MeV}^{-1}$ . Comparison of the best fitting spectrum of protons with the observational data is shown in Fig. 1. We see very good agreement between the calculated spectrum and the data. The minimum  $\chi^2$  value is about 24 for 72 degree of freedom (dof).

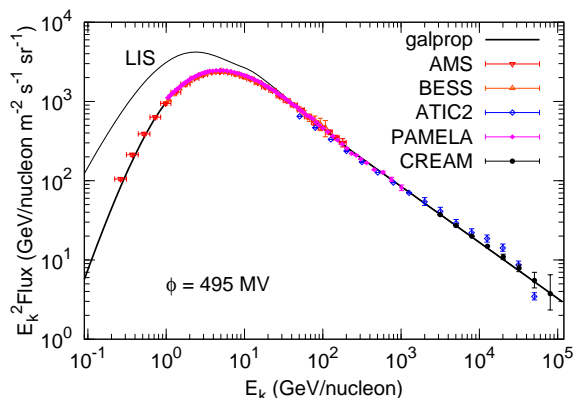


FIG. 1: Proton spectrum derived through fitting PAMELA and CREAM data. References of the proton data: AMS [46], BESS [47], ATIC2 [19], PAMELA [20] and CREAM [21].

Since the observational period of protons by PAMELA is almost the same with that of electrons by PAMELA and positrons by AMS-02, we should expect a common modulation amplitude for these particles (besides the charge-sign dependent effect). Therefore we employ a prior on the modulation potential  $\phi = 500 \pm 53$  MV comes from the fit of the proton data.

We first fix the electron second break energy  $p_{\text{br},2}^e$  at 230 GeV, same as that of protons. The best fitting results of the positron fraction and electron spectrum are shown in Fig. 2. The fitting parameters and the  $\chi^2$  value are presented in Table I. Compared with the case without spectral hardening of the primary electrons (Paper I), the fitting is indeed improved. The  $\chi^2$  value decrease

from  $\sim 280$  to 235 with one more parameter. However, the overall fitting is still not satisfactory. We can see from Fig. 2 that when AMS-02 data are well reproduced, the model expectation is lower than the Fermi data, which is similar with the findings in Paper I.

We then relax the break momentum of the electrons and redo the fit. In this case we find the improvement is significantly, as shown in Fig. 3. The parameters are also given in Table I. The minimum  $\chi^2$  value over dof is about 1.0, which implies a rather good fitting. However, the break momentum  $p_{\text{br},2}^e$  is required to be about 45 GeV, which is significantly smaller than that of the nuclei. The difference of the spectral indices below and above  $p_{\text{br},2}^e$  is about 0.3. As a comparison, such a value is measured to be  $\sim 0.2$  for protons and  $\sim 0.3$  for Helium [20]. Note, for the fit of proton spectrum in a wider energy range, as shown in Fig. 1, the spectral difference is only about 0.1.

It is also possible that the spectral hardening is not a break but a smooth hardening instead, as shown in many models [23, 27]. We may use a log-parabolic function to approximate the smooth hardening of the electron spectrum. Fig. 4 presents the results of the fit with log-parabolic shape of the primary electron spectrum. We find the fit is also improved, with the minimum  $\chi^2$  value slightly larger than that with  $p_{\text{br},2}^e$  free. The fitting parameters are given in Table I.

From above we see that including a spectral hardening of the primary electron spectrum, both the PAMELA, AMS-02 and Fermi data can be well fitted with a single component of the extra sources. It is a natural expectation that there is a hardening in the primary electron spectrum, given the observed hardening of the CR nuclei. However, the position of the break might be different from that of nuclei. It is a problem needs to be further understood theoretically. If the hardening of the primary electron spectrum can be confirmed, it would be important to understand the origin and acceleration of the Galactic CRs. Since AMS-02 could measure the pure electron spectrum with much higher precision than PAMELA, we give the expected pure electron spectra in Fig. 5 for the above three cases of the hardening. The future AMS-02 data may test the existence and detailed shape of the primary electron spectrum.

Finally we discuss the DM annihilation as the sources of the  $e^\pm$ . The annihilation final states are assumed to be  $\mu^+\mu^-$  and  $\tau^+\tau^-$ . The primary electron spectrum is parameterized with Eq. (1), and  $p_{\text{br},2}^e$  is allowed to be free in the fit. The fitting results are shown in Figs. 6 and 7, for  $\mu^+\mu^-$  and  $\tau^+\tau^-$  final states respectively. The fitting parameters are compiled in Table II. It is shown that the DM models can give comparable fittings to the data compared with pulsars. The break momentum of the primary electrons,  $p_{\text{br},2}^e$  is also similar with that derived in the pulsar scenario, and is smaller than  $p_{\text{br},2}^p \approx 230$  GeV.

The  $1\sigma$  and  $2\sigma$  favored regions on the  $m_\chi - \langle\sigma v\rangle$  parameter plane are given in Fig. 8. For  $\mu^+\mu^-$  channel DM

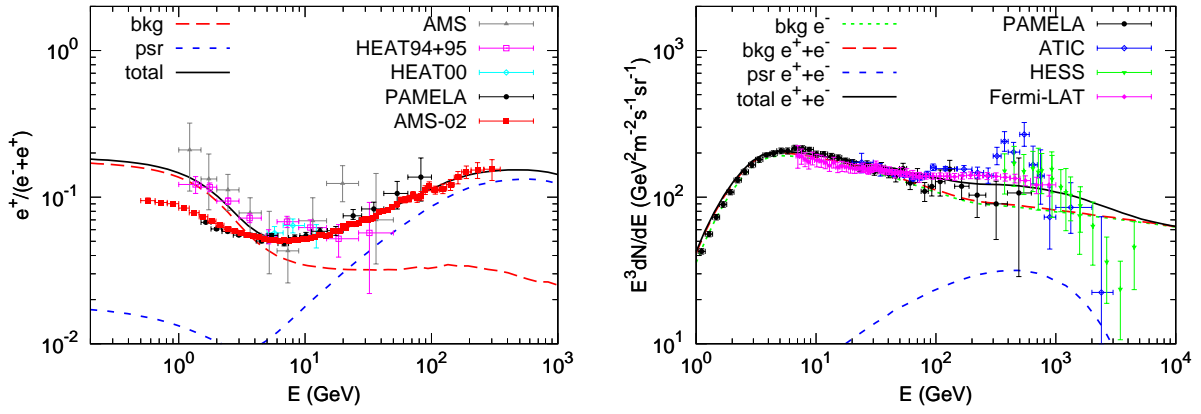


FIG. 2: The positron fraction (left) and electron spectra (right) for the background together with a pulsar-like component of the exotic  $e^\pm$ . The high energy hardening of the primary electron spectrum is approximated with a broken power-law and the break momentum  $p_{br,2}^e$  is fixed to be  $\sim 230$  GeV. References of the data: positron fraction — AMS01 [48], HEAT94+95 [49], HEAT00 [50], PAMELA [2], AMS-02 [1]; electron — PAMELA [9], ATIC [51], HESS [12, 13], Fermi-LAT [10].

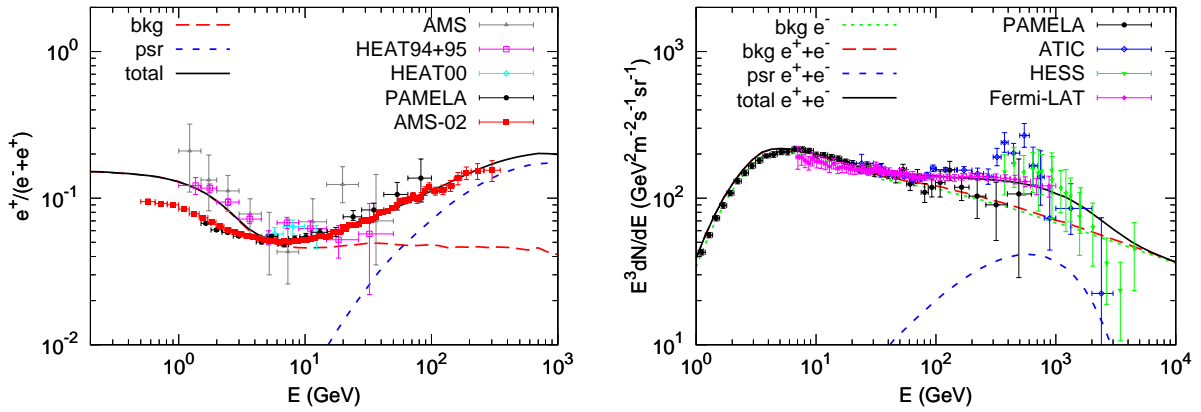


FIG. 3: Same as Fig. 2 but the high energy break of the electrons is relaxed in the fit.

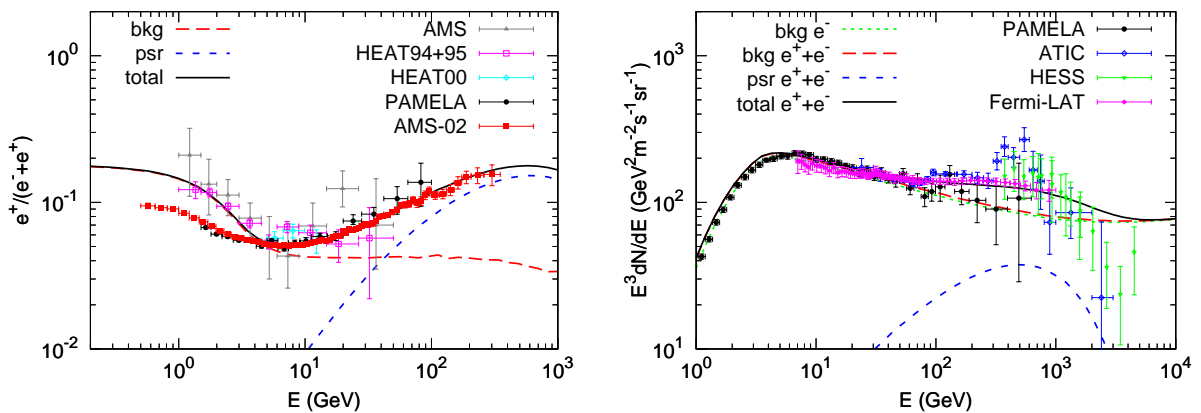


FIG. 4: Same as Fig. 3 but for a log-parabolic approximation of the spectral hardening of the primary electron spectrum.

with mass  $0.8\text{--}1.5$  TeV is favored, while for  $\tau^+\tau^-$  channel the mass is obtained to be  $2\text{--}4$  TeV. The boost factor of the annihilation cross section compared with the natural

value to give the proper relic density is about hundred to thousand. Such results do not differ much from the ones obtained through fitting the PAMELA positron fraction

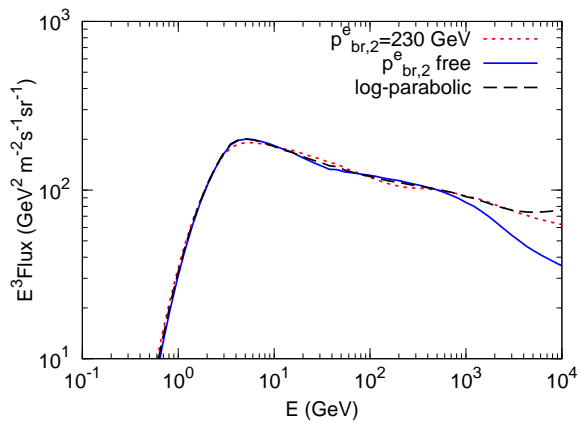


FIG. 5: Expected total fluxes of the pure electrons for the three fits corresponding to Figs. 2 - 4.

and the Fermi/HESS  $e^\pm$  data [41].

The exclusion limits on the DM annihilation into  $\mu^+\mu^-$  and  $\tau^+\tau^-$  pairs by  $\gamma$ -rays from the Galactic center (thin lines, [52]) and the dwarf galaxies (thick lines, [53]) are also plotted in Fig. 8. The results show that for the  $\tau^+\tau^-$  channel the Fermi  $\gamma$ -rays always give very strong constraints on the annihilation cross section. The constraints for the  $\mu^+\mu^-$  channel is weaker. The Galactic center  $\gamma$ -rays tend to exclude the parameter space to explain the  $e^\pm$  excesses. However it may suffer from the uncertainties of the density profile of DM in the halo center. The more robust limits from the dwarf galaxies can not exclude the favored parameter region.

#### IV. CONCLUSION AND DISCUSSION

The study of the highly precise data of positron fraction in CRs reported by AMS-02, as well as the pure electron spectrum measured by PAMELA and the total  $e^\pm$  spectra measured by Fermi and HESS, shows that it is difficult to use a single component of the extra sources to explain the  $e^\pm$  excesses (Paper I, [14]). In this work we show that an additional break of the primary electron spectrum can improve the fit significantly. The best fitting break momentum is about 40 – 50 GeV and the spectral difference  $\gamma_2 - \gamma_1$  is  $\sim 0.3 - 0.4$ . As a comparison, the break momentum of protons is about 230 GeV, and the spectral difference is  $\sim 0.1$ . The hardening behavior

of the electron spectrum is different from that of nuclei, which makes the understanding of the fine structures of the CR spectra non-trivial.

The different behaviors of the spectral hardening between nuclei and electrons are probably due to the fact that high energy electrons should come from nearby regions, and less number of relevant sources leads to larger fluctuations of the electron spectrum than that of nuclei. It is also possible that, if one or several nearby sources are responsible to the spectral hardening, the accelerated electron-to-proton ratio is higher for these sources.

In the presence of a hardening of the primary electron spectrum, both the pulsar and DM scenarios can give comparable fit to the data. However, the DM scenario are strongly constrained by the  $\gamma$ -rays, especially for the tauon final state. We would like to point out that it will be equivalent to take the harder part of the electron spectrum and to drop the constraints from the PAMELA electron data. In such ways both the AMS-02 positron fraction and Fermi total  $e^\pm$  spectrum can be fitted simultaneously.

The AMS-02 will measure the electron spectrum with high precision in the near future. Whether there is a hardening in the electron spectrum or a lower  $e^\pm$  total spectrum than Fermi will soon be answered by AMS-02.

#### Appendix A: Results of the background positrons and electrons

For the convenience of use we tabulate the fluxes of the background positrons and electrons calculated with the best fitting parameters of the pulsar models in Table III. For DM models the results have little difference. Note for background positrons an additional factor  $c_{e^+}$  as given in Table I needs to be multiplied. Here the local interstellar fluxes are given. If one wants to better reproduce the low energy electron spectrum, the solar modulation with modulation potential given in Table I is necessary.

#### Acknowledgments

This work is supported by 973 Program under Grant No. 2013CB837000 and the National Natural Science Foundation of China under Grant Nos. 11075169, 11105155.

[1] M. Aguilar, et al., Phys. Rev. Lett. **110**, 141102 (2013).  
 [2] O. Adriani, et al., Nature **458**, 607 (2009), 0810.4995.  
 [3] O. Adriani, et al., Astroparticle Physics **34**, 1 (2010), 1001.3522.  
 [4] M. Ackermann, et al., Phys. Rev. Lett. **108**, 011103 (2012), 1109.0521.  
 [5] T. Linden and S. Profumo, Astrophys. J. **772**, 18 (2013),

1304.1791.  
 [6] J. Kopp, Phys. Rev. D **88**, 076013 (2013), 1304.1184.  
 [7] A. De Simone, A. Riotto, and W. Xue, J. Cosmol. Astropart. Phys. **5**, 003 (2013), 1304.1336.  
 [8] M. Ibe, S. Iwamoto, S. Matsumoto, T. Moroi, and N. Yokozaki, Journal of High Energy Physics **8**, 29 (2013), 1304.1483.

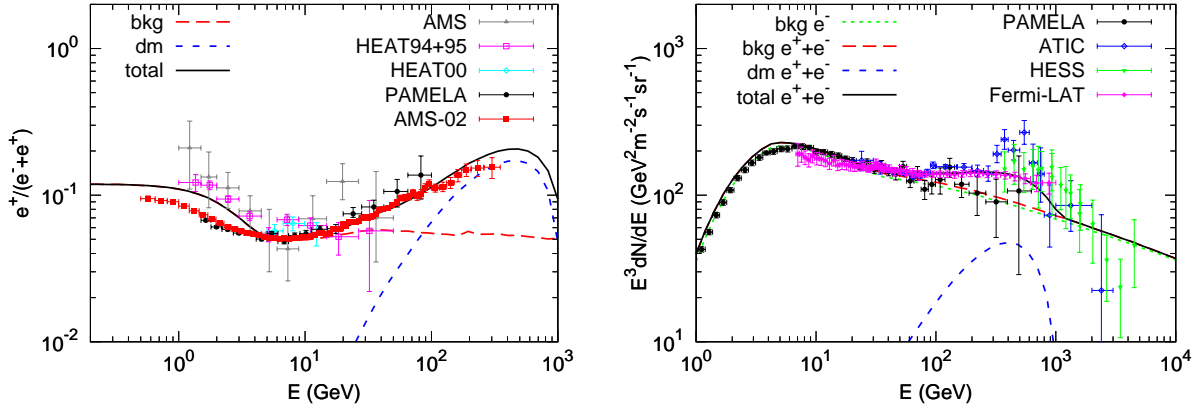


FIG. 6: Same as Fig. 3 but for the DM annihilation into a pair of muons as the extra source of the positrons and electron.

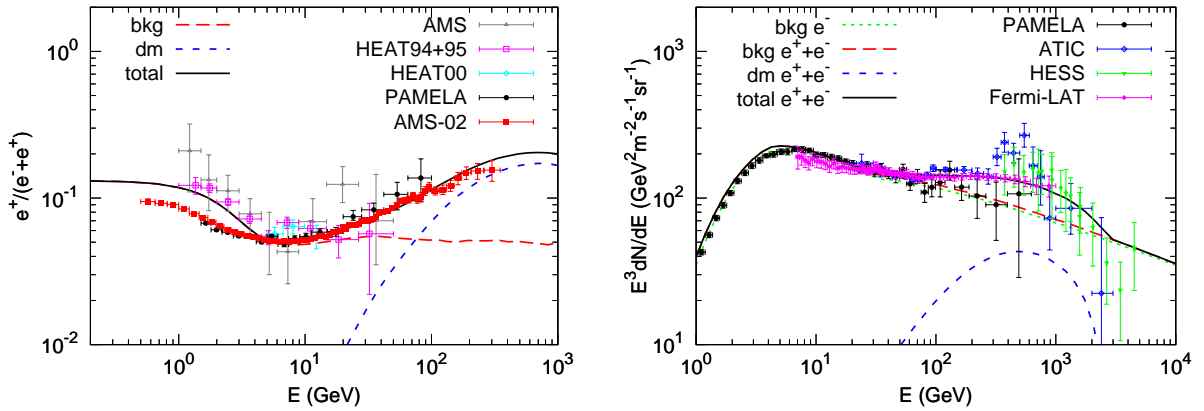


FIG. 7: Same as Fig. 3 but for the DM annihilation into a pair of tauons as the extra source of the positrons and electron.

TABLE I: Fitting results of pulsar-like model for different primary electron spectra

$\chi^2_{\min}/\text{dof}$	$p_{\text{br},2}^e = 230 \text{ GeV}$ 235.3/150		$p_{\text{br},2}^e$ free 152.5/149		log-parabolic 171.4/150	
	best	mean	best	mean	best	mean
$\log(A_e^a)$	-8.971	-8.973 $\pm$ 0.005	-8.978	-8.977 $\pm$ 0.007	-8.980	-8.976 $\pm$ 0.005
$\gamma_0$	1.504	1.515 $\pm$ 0.015	1.624	1.606 $\pm$ 0.054	1.536	1.558 $\pm$ 0.042
$\log(p_{\text{br},1}^e/\text{MeV})$	3.587	3.592 $\pm$ 0.021	3.625	3.622 $\pm$ 0.030	3.630	3.633 $\pm$ 0.021
$\gamma_1$	2.683	2.683 $\pm$ 0.011	2.851	2.839 $\pm$ 0.023	3.252	3.283 $\pm$ 0.056
$\log(p_{\text{br},2}^e/\text{MeV})$	—	—	4.630	4.638 $\pm$ 0.068	—	—
$\gamma_2$	2.368	2.370 $\pm$ 0.031	2.536	2.533 $\pm$ 0.025	0.101	0.106 $\pm$ 0.009
$\log(A_{\text{psr}}^b)$	-25.036	-25.066 $\pm$ 0.168	-27.406	-26.981 $\pm$ 0.397	-26.502	-26.547 $\pm$ 0.359
$\alpha$	1.881	1.875 $\pm$ 0.034	1.434	1.516 $\pm$ 0.077	1.599	1.592 $\pm$ 0.071
$\log(p_c/\text{MeV})$	6.242	6.280 $\pm$ 0.103	6.022	6.074 $\pm$ 0.087	6.053	6.043 $\pm$ 0.095
$c_{e+}$	1.460	1.464 $\pm$ 0.077	2.244	2.177 $\pm$ 0.104	1.916	1.972 $\pm$ 0.103
$\phi/\text{MV}$	561	558 $\pm$ 29	735	716 $\pm$ 37	629	653 $\pm$ 36

<sup>a</sup>Normalization at 25 GeV in unit of  $\text{cm}^{-2}\text{s}^{-1}\text{sr}^{-1}\text{MeV}^{-1}$ .

<sup>b</sup>Normalization at 1 MeV in unit of  $\text{cm}^{-3}\text{s}^{-1}\text{MeV}^{-1}$ .

[9] O. Adriani, et al., Phys. Rev. Lett. **106**, 201101 (2011).  
[10] M. Ackermann, et al., Phys. Rev. D **82**, 092004 (2010).

[11] A. A. Abdo, et al., Phys. Rev. Lett. **102**, 181101 (2009), 0905.0025.

TABLE II: Fitting results of DM annihilation model

$\chi^2_{\min}/\text{dof}$	$\mu^+\mu^-$		$\tau^+\tau^-$	
	186.6/150		160.5/150	
parameters	best	mean	best	mean
$\log(A_e^a)$	-8.970	$-8.970 \pm 0.007$	-8.979	$-8.978 \pm 0.008$
$\gamma_0$	1.766	$1.768 \pm 0.039$	1.718	$1.712 \pm 0.046$
$\log(p_{\text{br},1}^e/\text{MeV})$	3.690	$3.688 \pm 0.026$	3.678	$3.671 \pm 0.027$
$\gamma_1$	2.938	$2.943 \pm 0.012$	2.925	$2.921 \pm 0.014$
$\log(p_{\text{br},2}^e/\text{MeV})$	4.611	$4.597 \pm 0.041$	4.554	$4.563 \pm 0.048$
$\gamma_2$	2.541	$2.547 \pm 0.023$	2.547	$2.548 \pm 0.019$
$\log(m_\chi/\text{GeV})$	3.063	$3.071 \pm 0.061$	3.486	$3.451 \pm 0.056$
$\log(\langle\sigma v\rangle/\text{cm}^3\text{s}^{-1})$	-22.897	$-22.885 \pm 0.105$	-22.043	$-22.104 \pm 0.090$
$c_{e+}$	2.683	$2.687 \pm 0.059$	2.524	$2.522 \pm 0.067$
$\phi/\text{MV}$	839	$849 \pm 30$	796	$796 \pm 32$

<sup>a</sup>Normalization at 25 GeV in unit of  $\text{cm}^{-2}\text{s}^{-1}\text{sr}^{-1}\text{MeV}^{-1}$ .

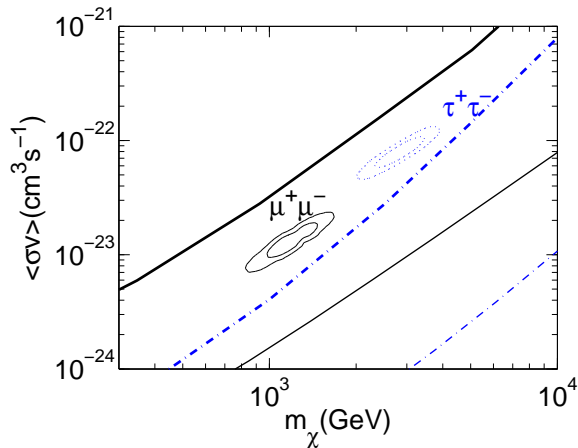


FIG. 8:  $1\sigma$  and  $2\sigma$  parameter regions on the  $m_\chi - \langle\sigma v\rangle$  plane for the DM annihilation scenario. The lines show the 95% upper limit of Fermi  $\gamma$ -ray observations of the Galactic center (thin lines, with different normalization of the local density corrected, [52]) and dwarf galaxies (thick lines, [53]) for  $\mu^+\mu^-$  (black solid) and  $\tau^+\tau^-$  (blue dashed-dotted) channels respectively.

[12] F. Aharonian, et al., Phys. Rev. Lett. **101**, 261104 (2008), 0811.3894.  
[13] F. Aharonian, et al., Astron. Astrophys. **508**, 561 (2009), 0905.0105.  
[14] Q. Yuan, X.-J. Bi, G.-M. Chen, Y.-Q. Guo, S.-J. Lin, and X. Zhang, ArXiv e-prints:1304.1482 (2013), 1304.1482.  
[15] AMS-02 collaboration, in *International Cosmic Ray Conference* (<http://www.ams02.org/2013/07/new-results-from-ams-presented-at-icrc-2013/>, 2013).  
[16] I. Cholis and D. Hooper, Phys. Rev. D **88**, 023013 (2013), 1304.1840.  
[17] H.-B. Jin, Y.-L. Wu, and Y.-F. Zhou, J. Cosmol. Astropart. Phys. **11**, 026 (2013), 1304.1997.  
[18] L. Feng, R.-Z. Yang, H.-N. He, T.-K. Dong, Y.-Z. Fan, and J. Chang, Physics Letters B **728**, 250 (2014),

1303.0530.  
[19] A. D. Panov, et al., Bulletin of the Russian Academy of Science, Phys. **71**, 494 (2007), astro-ph/0612377.  
[20] O. Adriani, et al., Science **332**, 69 (2011), 1103.4055.  
[21] H. S. Ahn, et al., Astrophys. J. Lett. **714**, L89 (2010), 1004.1123.  
[22] V. I. Zatsepin and N. V. Sokolskaya, Astron. Astrophys. **458**, 1 (2006), astro-ph/0601475.  
[23] Q. Yuan, B. Zhang, and X.-J. Bi, Phys. Rev. D **84**, 043002 (2011), 1104.3357.  
[24] A. D. Erlykin and A. W. Wolfendale, Astroparticle Physics **35**, 449 (2012), 1111.3191.  
[25] S. Thoudam and J. R. Hörandel, Mon. Not. Roy. Astron. Soc. **421**, 1209 (2012), 1112.3020.  
[26] G. Bernard, T. Delahaye, Y.-Y. Keum, W. Liu, P. Salati, and R. Taillet, Astron. Astrophys. **555**, A48 (2013), 1207.4670.  
[27] V. Ptuskin, V. Zirakashvili, and E.-S. Seo, Astrophys. J. **763**, 47 (2013), 1212.0381.  
[28] A. E. Vladimirov, G. Jóhannesson, I. V. Moskalenko, and T. A. Porter, Astrophys. J. **752**, 68 (2012), 1108.1023.  
[29] N. Tomassetti, Astrophys. J. Lett. **752**, L13 (2012), 1204.4492.  
[30] J. Liu, Q. Yuan, X.-J. Bi, H. Li, and X. Zhang, Phys. Rev. D **85**, 043507 (2012), 1106.3882.  
[31] A. W. Strong and I. V. Moskalenko, Astrophys. J. **509**, 212 (1998), astro-ph/9807150.  
[32] A. Lewis and S. Bridle, Phys. Rev. D **66**, 103511 (2002), astro-ph/0205436.  
[33] S. J. Lin, C. F. Cai, and et al., in preparation (2013).  
[34] T. Kamae, N. Karlsson, T. Mizuno, T. Abe, and T. Koi, Astrophys. J. **647**, 692 (2006), astro-ph/0605581.  
[35] Y.-Z. Fan, B. Zhang, and J. Chang, International Journal of Modern Physics D **19**, 2011 (2010), 1008.4646.  
[36] P. D. Serpico, Astroparticle Physics **39**, 2 (2012), 1108.4827.  
[37] D. J. Thompson, et al., Astrophys. J. **436**, 229 (1994).  
[38] D. R. Lorimer, in *Young Neutron Stars and Their Environments*, edited by F. Camilo & B. M. Gaensler (2004), vol. 218 of *IAU Symposium*, p. 105.  
[39] M. Cirelli, M. Kadastik, M. Raidal, and A. Strumia, Nuclear Physics B **813**, 1 (2009), 0809.2409.

TABLE III: Local interstellar fluxes of the background positrons and electrons

$E(\text{GeV})$	$E^2 F(\text{GeV m}^{-2} \text{s}^{-1} \text{sr}^{-1})$			
	$e^+$	$e^-(p_{\text{br},2}^e = 230 \text{ GeV})$	$e^-(p_{\text{br},2}^e \text{ free})$	$e^-(\text{log-parabolic})$
1.0000E - 01	1.0085E + 01	6.3746E + 01	1.2352E + 02	8.3203E + 01
1.2649E - 01	1.3343E + 01	8.1775E + 01	1.5669E + 02	1.0641E + 02
1.5999E - 01	1.6996E + 01	1.0265E + 02	1.9495E + 02	1.3312E + 02
2.0236E - 01	2.0939E + 01	1.2667E + 02	2.3747E + 02	1.6386E + 02
2.5595E - 01	2.4880E + 01	1.5278E + 02	2.8359E + 02	1.9708E + 02
3.2375E - 01	2.8681E + 01	1.8086E + 02	3.3104E + 02	2.3162E + 02
4.0949E - 01	3.2094E + 01	2.0769E + 02	3.7547E + 02	2.6486E + 02
5.1795E - 01	3.4604E + 01	2.3058E + 02	4.1054E + 02	2.9230E + 02
6.5513E - 01	3.5781E + 01	2.4683E + 02	4.3241E + 02	3.1091E + 02
8.2864E - 01	3.5182E + 01	2.5437E + 02	4.3443E + 02	3.1729E + 02
1.0481E + 00	3.2114E + 01	2.4778E + 02	4.1198E + 02	3.0636E + 02
1.3257E + 00	2.7285E + 01	2.3049E + 02	3.7033E + 02	2.8109E + 02
1.6768E + 00	2.1238E + 01	2.0411E + 02	3.1604E + 02	2.4608E + 02
2.1210E + 00	1.4943E + 01	1.7304E + 02	2.5584E + 02	2.0548E + 02
2.6827E + 00	9.6236E + 00	1.4278E + 02	2.0096E + 02	1.6662E + 02
3.3932E + 00	5.7713E + 00	1.1408E + 02	1.5456E + 02	1.3231E + 02
4.2919E + 00	3.3159E + 00	8.6156E + 01	1.1499E + 02	1.0119E + 02
5.4287E + 00	1.9367E + 00	6.0846E + 01	7.8414E + 01	7.0057E + 01
6.8665E + 00	1.1805E + 00	4.2413E + 01	5.2323E + 01	4.7256E + 01
8.6851E + 00	7.5988E - 01	2.9862E + 01	3.5204E + 01	3.2186E + 01
1.0985E + 01	5.1230E - 01	2.1185E + 01	2.3941E + 01	2.2173E + 01
1.3895E + 01	3.5859E - 01	1.5280E + 01	1.6600E + 01	1.5669E + 01
1.7575E + 01	2.5470E - 01	1.1079E + 01	1.1644E + 01	1.1211E + 01
2.2230E + 01	1.8315E - 01	8.0717E + 00	8.1879E + 00	8.0348E + 00
2.8118E + 01	1.3379E - 01	5.9131E + 00	5.8546E + 00	5.8577E + 00
3.5565E + 01	9.7597E - 02	4.3215E + 00	4.2067E + 00	4.2699E + 00
4.4984E + 01	7.3397E - 02	3.2332E + 00	3.1587E + 00	3.2056E + 00
5.6899E + 01	5.3549E - 02	2.3330E + 00	2.3430E + 00	2.3364E + 00
7.1969E + 01	3.9877E - 02	1.7106E + 00	1.7699E + 00	1.7348E + 00
9.1030E + 01	2.9733E - 02	1.2613E + 00	1.3334E + 00	1.2936E + 00
1.1514E + 02	2.2265E - 02	9.3209E - 01	1.0104E + 00	9.6957E - 01
1.4563E + 02	1.6558E - 02	6.8757E - 01	7.5661E - 01	7.2384E - 01
1.8421E + 02	1.2349E - 02	5.1494E - 01	5.6947E - 01	5.4575E - 01
2.3300E + 02	9.2290E - 03	3.9036E - 01	4.2686E - 01	4.1269E - 01
2.9471E + 02	6.8405E - 03	3.0270E - 01	3.1791E - 01	3.1194E - 01
3.7276E + 02	5.0884E - 03	2.3532E - 01	2.3806E - 01	2.3722E - 01
4.7149E + 02	3.7641E - 03	1.8276E - 01	1.7733E - 01	1.8072E - 01
5.9636E + 02	2.7641E - 03	1.4101E - 01	1.3197E - 01	1.3743E - 01
7.5431E + 02	2.0308E - 03	1.0876E - 01	9.7899E - 02	1.0576E - 01
9.5410E + 02	1.4738E - 03	8.3842E - 02	7.2376E - 02	8.1243E - 02
1.2068E + 03	1.0837E - 03	6.5258E - 02	5.4198E - 02	6.3344E - 02
1.5264E + 03	7.7609E - 04	5.0293E - 02	4.0077E - 02	4.9167E - 02
1.9307E + 03	5.5115E - 04	3.8733E - 02	2.9646E - 02	3.8295E - 02
2.4421E + 03	3.8831E - 04	2.9902E - 02	2.1981E - 02	3.0025E - 02
3.0888E + 03	2.7001E - 04	2.3065E - 02	1.6307E - 02	2.3726E - 02
3.9069E + 03	1.8373E - 04	1.7810E - 02	1.2022E - 02	1.8746E - 02
4.9417E + 03	1.2265E - 04	1.3675E - 02	8.8979E - 03	1.4890E - 02
6.2506E + 03	8.0038E - 05	1.0560E - 02	6.5895E - 03	1.1899E - 02
7.9060E + 03	5.0413E - 05	8.1294E - 03	4.8656E - 03	9.5347E - 03
1.0000E + 04	3.0695E - 05	6.2648E - 03	3.5951E - 03	7.6744E - 03



- [40] P. F. Yin, Q. Yuan, J. Liu, J. Zhang, X. J. Bi, S. H. Zhu, and X. M. Zhang, *Phys. Rev. D* **79**, 023512 (2009), 0811.0176.
- [41] P. Meade, M. Papucci, A. Strumia, and T. Volansky, *Nuclear Physics B* **831**, 178 (2010), 0905.0480.
- [42] J. F. Navarro, C. S. Frenk, and S. D. M. White, *Astrophys. J.* **490**, 493 (1997), astro-ph/9611107.
- [43] L. J. Gleeson and W. I. Axford, *Astrophys. J.* **154**, 1011 (1968).
- [44] L. Maccione, *Phys. Rev. Lett.* **110**, 081101 (2013), 1211.6905.
- [45] S. Della Torre, et al., *Advances in Space Research* **49**, 1587 (2012).
- [46] J. Alcaraz, et al., *Phys. Lett. B* **490**, 27 (2000).
- [47] T. Sanuki, et al., *Astrophys. J.* **545**, 1135 (2000), astro-ph/0002481.
- [48] M. Aguilar, et al., *Phys. Lett. B* **646**, 145 (2007), astro-ph/0703154.
- [49] S. W. Barwick, et al., *Astrophys. J. Lett.* **482**, L191 (1997), astro-ph/9703192.
- [50] S. Coutu, et al., in *International Cosmic Ray Conference* (2001), vol. 5 of *International Cosmic Ray Conference*, p. 1687.
- [51] J. Chang, et al., *Nature* **456**, 362 (2008).
- [52] X. Huang, Q. Yuan, P.-F. Yin, X.-J. Bi, and X. Chen, *J. Cosmol. Astropart. Phys.* **11**, 048 (2012), 1208.0267.
- [53] A. Drlica-Wagner, in *Fermi Symposium 2012* (2012).